

Calibration Improvements Expand Filterscope Diagnostic Use

J. L. Herfindal,^{1, a)} E. A. Unterberg,¹ K. M. Davda,² E. W. Garren,¹ M. Groth,³ F. Scotti,⁴ A. C. Sontag,⁵ D. D. Truong,⁶ and R. S. Wilcox¹

¹⁾ Oak Ridge National Laboratory, Oak Ridge, TN 37831, U.S.A

²⁾ University of Tennessee, Knoxville, TN 37996, U.S.A

³⁾ Aalto University, Espoo, Finland

⁴⁾ Lawrence Livermore National Laboratory, Livermore, CA 94550, U.S.A

⁵⁾ University of Wisconsin Madison, Madison, WI 53706, U.S.A

⁶⁾ Sandia National Laboratory, Livermore, CA 94550, U.S.A

(Dated: 16 January 2024)

The filterscope diagnostic on DIII-D utilizes photomultiplier tubes to measure visible light emission from the plasma. The system has undergone a substantial upgrade since previous attempts to cross-calibrate the filterscope with other spectroscopic diagnostics were unsuccessful. The optics now utilize a dichroic mirror to initially split the light at nearly 99% transmission or reflectance for light below or above 550 nm. This allows the system to measure D_α emission without degrading visible light emission from the plasma for wavelengths below 550 nm (to measure D_β , D_γ , W-I, C-III, etc.). Additional optimization of the optical components and calibration techniques reduce the error in the signal up to 10% in some channels compared to previous methods. Cross-calibration measurements with two other high resolution spectroscopic diagnostics now show excellent agreement for the first time. This expands the capabilities of the filterscope system allowing measurement of divertor detachment, emission profiles, edge-localized mode (ELM) behavior, plasma-wall interactions. It also enables direct comparisons against calculations from boundary plasma simulations. These were not possible before.

I. INTRODUCTION

The filterscope (FS) diagnostic is a low-cost spectroscopy system that uses band-pass filters to measure specific regions of the electromagnetic spectrum with a high time resolution (usually 50 kHz or higher). Similar diagnostics used to measure calibrated charge state radiation has been around since the 1980s in PDX¹ and later in Alcator-C², JET³, TFTR⁴, and DIII-D⁵ until ORNL developed the general FS design.⁶ Implementation typically includes view chords observing specific regions of interest or fan-like arrays covering tangentially across the plasma and/or the divertor regions. Band-pass filters are selected to monitor line radiation or continuum radiation which is measured through photomultiplier tubes. The fast line radiation measurements are extremely useful to determine several plasma phenomena. For example, calibrated D_α measurements are commonly used to detect and classify Edge Localized Mode (ELM) behavior.^{7,8} Splitting the light from one view chord to measure several different charge states simultaneously can identify plasma detachment⁹, measure plasma edge conditions¹⁰, and help constrain plasma modeling codes. Recently, several filters have been added to compare simulations of neutral tungsten erosion rates against sputtering measurements using fast neutral tungsten (W-I, at 400.9 nm) spectroscopy.¹¹

Currently, filterscope diagnostics can be found on experiments worldwide such as DIII-D, KSTAR¹², JET, W7-X¹³, and EAST¹⁴. The filterscope diagnostic on

DIII-D underwent a significant upgrade to increase light throughput through new splitter designs, expanded capabilities to measure up to 96 channels simultaneously (from 64), and a complete overhaul of the calibration process resulting in excellent agreement with other high resolution spectroscopy diagnostics during a cross-calibration experiment for the first time.

This paper is organized as follows: Section II describes the hardware, upgraded optical components, and chord layout. Section III explains the filterscope calibration technique. Section IV shows the cross-calibration results with two other diagnostics. Section V summarizes the main conclusions.

II. HARDWARE

The basic design of a filterscope diagnostic is to have a light collection optic directed at the region of interest, focusing the light into a fiber optic. The light travels through the fiber optic and exits through a collimating lens. It is then split up to three times prior to passing through a band-pass filter to the Photo-Multiplier Tube (PMT). This allows simultaneous measurements of up to four different spectral lines per chord. A schematic of the general layout can be found in Refs. 6 and 15.

A. Viewing chords layout

The filterscope system on DIII-D currently has 36 viewing chords. The position of each viewing chord is measured with a coordinate measuring machine. Fig. 1 shows the arrangement of two filterscope fan arrays view-

^{a)} herfindaljl@ornl.gov

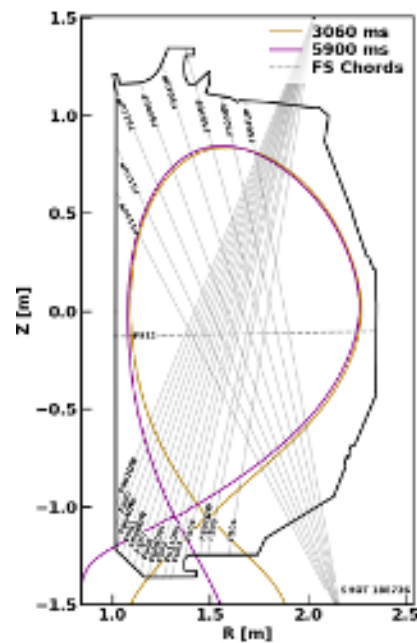


FIG. 1. Cross-section of the DIII-D vacuum vessel (black) superimposed with the center of cone-shaped viewing chords for the filterscope. A plasma separatrix flux surface is shown at two time slices (purple and goldenrod) showing the extent of the strike point sweep used for the cross calibration discussed in Sec. IV. An additional eight mid-plane views observing the plasma edge and four chords viewing the SAS divertor are not shown.

ing the upper and lower divertors. The upper divertor views are located at 150° toroidally and consist of eight chords (names ending in UP) while the lower divertor views are at 135° toroidally and make up 15 chords. A lens located outside of the vacuum vessel focuses the light upon an array of bare fiber optics. This arrangement results in conical views with elliptical spot sizes due to the non-normal angle of inclination with the tiles. An elliptical fit is performed on each chord where they intersect the wall and the upper and lower divertor views range from a 15.8 cm major and 7.79 cm minor diameter to a 5.7 cm major and 2.1 cm minor diameters ellipses.

The system also has a wide angle mid-plane view of the plasma located at 135° toroidally (dashed line in fig. 1). The viewing cone has a large opening angle of $\sim 20^\circ$ to observe the center post compared to a typical opening angle of $\sim 1^\circ$ for the other viewing chords. A description of eight additional mid-plane views observing the edge of the plasma can be found in Ref. 6.

Four additional views point directly into the new divertor configuration, the SAS-VW. One view is located below the machine at 30° toroidally looking straight up and three additional views have in-vessel optics viewing the tungsten-coated inboard side of the divertor (not shown).

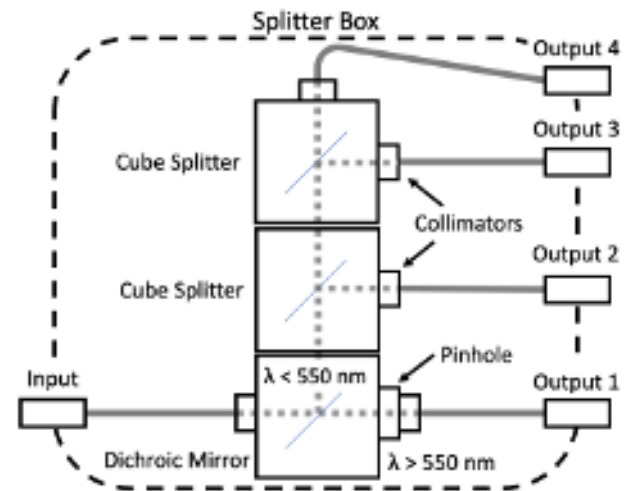


FIG. 2. New splitter box design used to split the incoming light from one viewing chord three times in order to measure four different spectral lines simultaneously. The light enters the box on the bottom-left to a fiber optic, exiting through a collimator to a dichroic mirror with a cut-on wavelength at 550 nm. The light above 550 nm passes through a pinhole to reduce intensity before going through another collimator to a fiber optic leaving the box. The light below 550 nm passes through additional cube splitters to further split the light prior to going through a collimator and leaving the box.

B. Splitter Optics

Light from the plasma travels from the machine hall approximately 35 m to the electrical annex where the optical splitter and electronics is located. There are two setup options for the optical splitter depending on filter inventory and physics needs of a particular channel. The first option is to bypass the splitter or have the light pass through a circular aperture to reduce intensity prior to reaching the band-pass filter and the PMT. Another option is to split the light up to three times depending on the view chord. The light could be split further to observe more spectral lines but is limited by the brightness of the atomic transition of interest.

The new splitter setup shown in fig. 2 consists of all off-the-shelf components and is enclosed in a rack mounted enclosure. The fiber optic from the machine attaches to the back of the box and the light enters the splitter box through a butt-jointed connector. The light then travels through another fiber optic leaving through a collimator (ThorLabs F950SMA-A) entering a dichroic mirror (ThorLabs DMLP550R) with a cut-on wavelength at 550 nm in the first stage. Channels observing faint lines, such as W-I, skip the butt-joint connector and the fibers from the machine hall are connected directly to the collimator inside of the splitter box.

The center wavelength of the dichroic mirror is chosen due to our specific setup where we observe D_α (656.1 nm) in every channel and do not want to lose signal strength to other lines of interest that are all primarily below

500 nm. The light above 550 nm then travels through a pinhole (with diameters ranging from 500 μm to 2000 μm) to decrease intensity prior to going through a collimator and a fiber to exit the box.

Light below 550 nm travels through one or two additional cube beam splitters (ThorLabs CCM1-BS013) to split the light prior to going through a collimator and leaving the box. The whole cube setup system uses the standard 30 mm cage cubes (ThorLabs CCM1) connected together to be light tight. The filterscope system uses low OH fiber optics with core diameters near 600 μm and numerical apertures (NA) ranging from 0.22 to 0.39. The collimator focal length is chosen to minimize beam divergence and light collection based off of the fiber optics on-hand and what is available for purchase off the shelf. Channels observing spectral lines near 400 nm use fiber optics with a thicker core (1000 μm , 0.5 NA) to maximize transmission at lower wavelengths.

C. Electronics and data storage

The DIII-D filterscope system uses a 6U VME form-factor chassis (ANSI/IEEE 1014-1987) consisting of eight modules (96 channels) with the fiber optic input connected directly to a mount that is aligned with the input of the PMT. Each PMT is held in a custom chassis holding the exit collimator, optical filter, operation amplifiers, and analog electronics to the data acquisition system. PMTs from Hamamatsu (models H5783 and H10721) are still in use with the majority of them from the previous filterscope system. Each signal from the PMTs is amplified for output into the data acquisition system and has the ability to provide real-time output of the filterscope signal to use for alarm triggering or for input into plasma control algorithms. A PXI express based data acquisition system by National Instruments (NI) is used to control and store the data. The filterscope system consists of a PXIe chassis (NI PXIe-1085), a PXI control module (NI PXIe-8840), eight PXIe input/output modules (NI PXI-6250), and a digital input/output module (NI PXI-6509). The data for each shot is stored locally on Synology RS816 rack station with multiple SATA hard drives using MDSplus¹⁶ to store the data. The raw data is then pushed to the experimental tree at DIII-D prior to being calibrated (using the technique discussed in sec. III) then pushed to another tree for access to the end user. Calibration information such as the measured filter transmission, PMT gain curves, in-vessel calibration measurements, is stored for each discharge for every channel. A more detailed description of the hardware components is found in Ref. 15.

III. ABSOLUTE INTENSITY CALIBRATION

An important part of the filterscope diagnostic is the absolute calibration of the light observed within the

band-pass of each filter. A complete calibration depends on four components: (1) measurement of the chordal position within the machine, (2) accurate representation of the filter transmission, (3) in-vessel measurements using an absolutely calibrated light source, and (4) a representation of the PMT response to different applied voltages.

The positional mapping of each view chord is discussed in more detail in sec. II A and is typically done after any changes with the optics or after several experimental campaigns. In-vessel calibrations using an absolutely calibrated Labsphere in terms of Φ_{LS} (photons / (s cm² sr nm)) is done prior to and after each experimental campaign. The Labsphere is brought inside the vessel to characterize the entire optical path and the average signal, V_{cal} , with standard deviation is recorded for one PMT gain setting, G_{cal} .

Filters are measured prior to a run campaign using a 1.33 m McPherson model 209 Czerny Turner design spectrometer with a 16-channel Princeton Instruments PI-MAX4i intensified CCD camera (the multi-chord diverter spectrometer (MDS) diagnostic at DIII-D)¹⁷. The system has a spectral resolution of ~ 0.02 nm and is wavelength calibrated using a spectral lamp with known line radiation in the region of the band-pass of the filter to be measured. A light-tight filter holder setup is assembled using collimators with a fixed empty space between them (to fit the filter) and a background white light signal is measured. The filter is then placed in the setup and the signal is divided by the background signal to get the filter transmission.

The integration of the filter transmission and the lab-sphere radiance gives the inherent number, I_h :

$$I_h = \int \Phi_{\text{LS}}(\lambda) T_f(\lambda) d\lambda. \quad (1)$$

Previous filterscope calibrations (see Ref. 6) used a Gaussian function to approximate the filter transmission for the inherent number calculation. Using a Gaussian approximation results in a larger inherent number, up to $\sim 10\%$, due to the boxcar-like transmission function for the current filter compared to previous Gaussian-like filter transmission. This would directly translate to an artificially increased calibrated signal (see eqn. 2) and is why a measured filter transmission is used.

The photon flux Φ (photons / (s cm² sr)) is given by:

$$\Phi = I_h \left[\frac{G_{\text{cal}} V_{\text{sig}}}{G_{\text{sig}} V_{\text{cal}}} \right], \quad (2)$$

where V_{sig} is the PMT voltage measured from the plasma during a discharge with a PMT gain of G_{sig} . PMT gain characterization is discussed in the next section.

A. PMT Gain Calibration

One of the big advantages that the filterscope diagnostic has over other spectral diagnostics is the ability

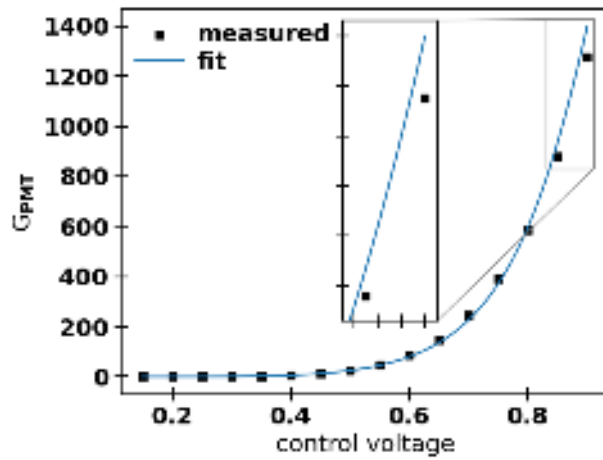


FIG. 3. Exponential gain curve of the PMT showing the measured values (solid squares) and a fit performed on those values (blue line). Previous techniques used the fitted values to calibrate the FS signals, introducing a systematic error as evident by the difference between the measured and fit function.

to exponentially increase the signal level without sacrificing time resolution. Fig. 3 shows a measured PMT gain curve, G_{PMT} , for one PMT in the filterscope system. The filterscope sends a reference voltage, called the control voltage, used by the internal high-voltage DC-DC converter that powers the PMT. The control voltage ranges from 0.05 to 1.0 V in increments of 0.05 V but is typically limited between 0.15 to 0.9 V for operations to ensure the PMT turns on and the signal to noise is sufficiently low.

Gain curves for each PMT (G_{PMT}) are measured after installation into the filterscope hardware. Measurement of G_{PMT} involves hooking up a light source to the PMT with a neutral density filter. The signal is recorded at each control voltage and the neutral density filter transmission is determined by recording signal levels at the same control voltage with the different neutral density filter setups. Signals are then scaled with respect to the lowest control voltage measured to generate the response curve (black squares) shown in fig. 3.

Calculation of the photon flux in eqn. 2 uses the measured G_{PMT} values to generate the quantities G_{cal} and G_{sig} at the control voltages used during the calibration and plasma measurement respectfully. Previous filterscope gain calibration curves fit the measured values to an exponential function with a fourth order polynomial in the exponent^{6,15} (blue line in fig. 3). The calibration programs would then use the fit to calculate G_{cal} and G_{sig} . However, the fits would routinely not match the measured G_{PMT} values at high control voltages as shown in the zoomed-in region in fig. 3. This mismatch is primarily due to PMT gain curves responding exponentially to the applied high voltage¹⁸, not the control voltage applied to the DC-DC converter. This source of systematic error has been eliminated from photon flux calculation

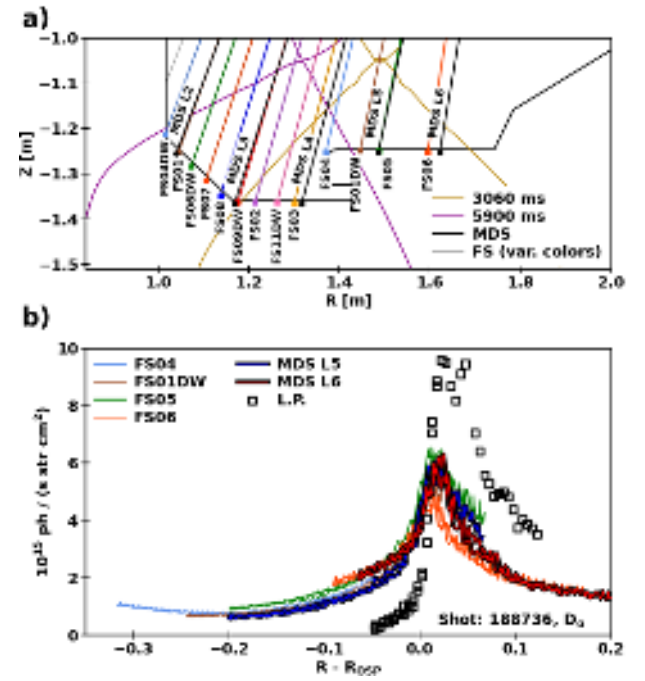


FIG. 4. (a) Zoomed-in view of the lower viewing filterscopes (various colors with square endpoints) and the MDS chords (black with circular endpoints) used in the cross-calibration. A plasma separatrix flux surface is shown at two time slices (purple and goldenrod) showing the extent of the strike point sweep used for the cross calibration discussed in Sec. IV. (b) Cross-calibration measurements showing the filterscope, MDS, and Langmuir probe diagnostics as the outer strike point swept across the line of sight of each view chord.

and the measured values (black squares in fig. 3) are used instead.

Repeatable and consistent PMT gain curves are an important factor to determine the validity of the calibrated signal. The gain curve, G_{PMT} , for four different PMTs was measured with a span of seven months and thousands of power cycles between the measurements. Each possible ratio of $G_{\text{CTRL}_i}/G_{\text{CTRL}_0}$ was computed for each base control voltage (G_{CTRL_0}). It was found that the highest average percent difference at a specific control voltage before and after thousands of power cycles was 3.5% with the lowest being 0.8%. On average, the repeatability of G_{PMT} is quite good, well within the typical margin of error of approximately 10% for the calibrated signal that takes into account the signal to noise ratio of the signal measured during a plasma discharge, errors in the absolute in-vessel calibration, G_{PMT} measurements, and filter transmission curves.

IV. CROSS-CALIBRATION

A strike-point sweep moves the main separatrix across the bottom (or top) of the machine several times during a single discharge. Fig. 1 and Fig. 4(a) shows the ex-

ment of a strike-point sweep used in the cross-calibration described in this section. The strike point (where the separatrix intersects the vessel tiles) starts outwards (goldenrod line) progressing inwards (purple line) then moves outwards once more. This results in an increase in measured D_α emission as the strike point intersects the view chord. Since there are two strike points, the cross-calibration comparisons are broken up into two plots depending on if the outer strike-point (OSP) or the inner strike-point (ISP) crossed the view chords. The OSP is the strike point in the right-hand side of fig. 4(a) (chords FS01DW to FS06) while the ISP is on the left-hand side (chords FS03 to FS04DW).

Fig. 4(b) shows the calibrated filterscope, MDS, and photon flux inferred from Langmuir probe (LP) signals during the cross-calibration sweep for the OSP chords. The x-axis is the difference between the radial strike point location and the radial chord position. It should be noted that the filterscope and MDS views do not directly overlap and measure the plasma at different toroidal locations. The filterscope views used in this cross-calibration are at 135 degrees while the MDS chords are at 150 degrees. Therefore, we would expect slight differences between the chords since the strike point has a different angle of inclination, flux expansion, and neutral recycling changes.

The MDS diagnostic, discussed briefly in sec. III, integrated counts for 1 ms at a time over a spectral range of 652 to 659 nm throughout the discharge. These counts are converted to photons using an absolute calibration and multiplied by a normalized D_α filter corresponding to the measured filter transmission curve in the nearest filterscope channel (FS05 for L5, FS06 for L6, etc.). The signal is then integrated for each time segment during the discharge in order to provide a direct comparison to the filterscope signals.

Deuteron flux determined through the LP diagnostic is shown in fig. 4(b) (black squares). LP radial profiles of the ion current perpendicular to the divertor target is quantitatively consistent with the profile of the deuteron flux when multiplied by a Johnson-Hinnov factor (inverse photon efficiency)¹⁹. Johnson-Hinnov factors ranging from 2 to 20 (typically around 19 when the strike point is on the LP) were calculated using Atomic Data Analysis Structure (ADAS²⁰) using the measured electron density and temperature values. The measured peak temperatures and densities were 30 eV and $1 \times 10^{19} \text{ m}^{-3}$, and are thus indicative of a low-recycling, ionizing plasma at the divertor plate.

Fig. 5(a) illustrates the ISP cross-calibrations during the same discharge. The x-axis is now the distance along the vessel wall, S , starting at the very bottom of the machine, $R = 1.43 \text{ m}$, $z = -1.38 \text{ m}$, progressing inboard (to the left in Fig. 1) in order to account for the different angled surfaces as you reach the inside of the machine.

Fig. 5(b) shows another discharge observing the C-III transition lines near 465 nm using the FS, MDS, and tangential TV (TangTV)²¹ diagnostics. The MDS data un-

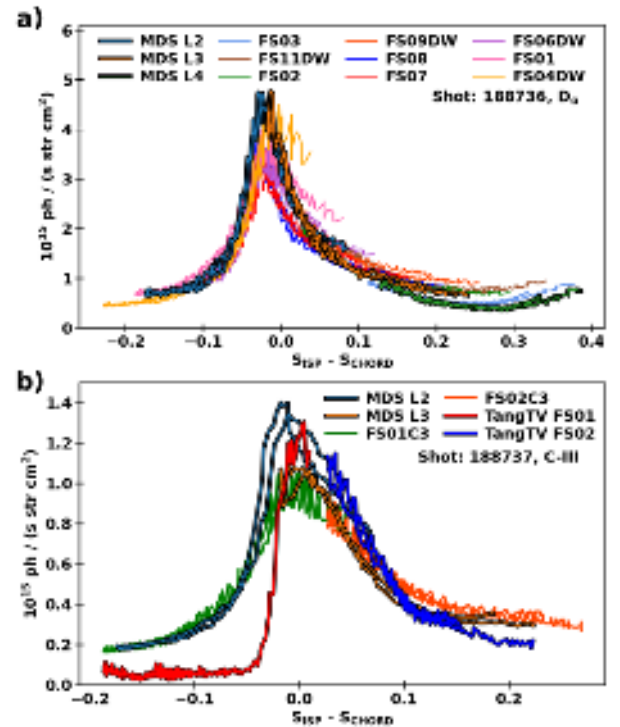


FIG. 5. Cross-calibration measurements showing the measurements of the filterscope, MDS, and TangTV diagnostics as the inner strike point swept across the line of sight of each view chord. The x-axis is a function of distance along the inner wall. D_α measurements are shown in (a) and the C-III transition lines near 465 nm are shown in (b).

derwent a similar treatment as discussed above to create a mock FS signal, using the normalized measured filter characterization curve corresponding to the nearest FS channel with a C-III filter (FS01 for L2 and FS02 for L3). Multiplication of the filter transmission curves is used to match the spectral observation range of both diagnostics. The filters used for comparison have a boxcar transmission curve centered at 465 nm with a bandpass of 2 nm (1.5 nm for D_α filters) with >95% transmission over the bandpass.

Filterscope data is compared with C-III brightness measured by TangTV cameras viewing the lower divertor through a narrow bandpass (2.1 nm) interference filter in fig. 5(b) (red and gray lines with a black outline). Local emissivities are obtained from tomographic inversion of the TangTV signal and a mock FS signal is then reproduced from the 2D emissivities through a synthetic diagnostic. Measurements match up well when the strike point is at the radial location where the FS chord intersects the lower divertor. TangTV only measures light in the lower divertor area therefore, line emission measured by the filterscopes outside of the lower divertor (e.g. upper SOL) is not represented in the TangTV measurement and would lead to a mismatch in regions away from the strike point.

V. CONCLUSIONS

An expanded filterscope system has been successfully designed and implemented on DIII-D. The diagnostic underwent a significant optical redesign, utilizing a dichroic mirror to extract D_α radiation without decreasing radiation due to wavelengths less than 550 nm. This technique results in higher signal levels for other commonly monitored line radiation such as D_β , D_γ , W-I, C-III, etc. Each portion of the updated calibration procedure has been tested and previous calibration techniques have been eliminated due to inaccuracy or introduction of systematic errors. The system shows good agreement with the MDS, LP, and TangTV diagnostics during a cross-calibration experiment for the first time. The absolute calibration of the system now enables direct comparisons against calculations from boundary plasma simulations which were not possible before.

ACKNOWLEDGMENTS

Discussions with Adam Mclean are gratefully acknowledged. This material is based upon work supported by the U.S. Department of Energy, Office of Science, Office of Fusion Energy Sciences, using the DIII-D National Fusion Facility, a DOE Office of Science user facility, under Award(s) DE-FC02-04ER54698, DE-AC05-00OR22725, DE-AC52-07NA27344, and DE-NA0003525. This manuscript has been authored by UT-Battelle, LLC, under contract DE-AC05-00OR22725 with the US Department of Energy (DOE). A.C. Sontag and K.M. Davda were supported through the ORNL DOE award number DE-AC05-00OR22725. The US government retains and the publisher, by accepting the article for publication, acknowledges that the US government retains a nonexclusive, paid-up, irrevocable, worldwide license to publish or reproduce the published form of this manuscript, or allow others to do so, for US government purposes. DOE will provide public access to these results of federally sponsored research in accordance with the DOE Public Access Plan (<http://energy.gov/downloads/doe-public-access-plan>).

Disclaimer: This report was prepared as an account of work sponsored by an agency of the United States Government. Neither the United States Government nor any agency thereof, nor any of their employees, makes any warranty, express or implied, or assumes any legal liability or responsibility for the accuracy, completeness, or usefulness of any information, apparatus, product, or process disclosed, or represents that its use would not infringe privately owned rights. Reference herein to any specific commercial product, process, or service by trade name, trademark, manufacturer, or otherwise does not necessarily constitute or imply its endorsement, recommendation, or favoring by the United States Government or any agency thereof. The views and opinions of authors expressed herein do not necessarily state or reflect those of the United States Government or any agency thereof.

REFERENCES

- ¹Kadota K, Otsuka M and Fujita J 1980 *Nuclear Fusion* **20** 209–212 URL <https://doi.org/10.1088/2F0029-5515/2F20%2F2%2F010>
- ²Foord M E, Marmar E S and Terry J L 1982 *Review of Scientific Instruments* **53** 1407–1409 (Preprint

- <https://doi.org/10.1063/1.1137176>) URL <https://doi.org/10.1063/1.1137176>
- ³Morgan P D, Behringer K H, Carolan P G, Forrest M J, Peacock N J and Stamp M F 1985 *Review of Scientific Instruments* **56** 862–864 (Preprint <https://doi.org/10.1063/1.1138074>) URL <https://doi.org/10.1063/1.1138074>
- ⁴Ramsey A T and Turner S L 1987 *Review of Scientific Instruments* **58** 1211–1220 (Preprint <https://doi.org/10.1063/1.1139441>) URL <https://doi.org/10.1063/1.1139441>
- ⁵Schissel D P, Stockdale R E, St John H and Tang W M 1988 *Phys. Fluids* **31** 3738
- ⁶Colchin R J, Hillis D L, Maingi R, Klepper C C and Brooks N H 2003 *Review of Scientific Instruments* **74** 2068–2070 (Preprint <https://doi.org/10.1063/1.1537038>) URL <https://doi.org/10.1063/1.1537038>
- ⁷Wade M R, Nazikian R, deGrassie J S, Evans T E, Ferraro N M, Moyer R A, Orlov D M, Buttery R J, Fenstermacher M E, Garofalo A M, Lanctot M A, McKee G R, Osborne T H, Shafer M A, Solomon W M, Snyder P B, Suttrop W, Wingen A, Unterberg E A and Zeng L 2015 *Nuclear Fusion* **55** 023002 URL <https://dx.doi.org/10.1088/0029-5515/55/2/023002>
- ⁸Wilcox R S, Baylor L R, Bortolon A, Knolker M, Lasnier C J, Shiraki D, Bykov I, Chrystal C, Scotti F, Paz-Soldan C and Wingen A 2022 *Nuclear Fusion* **62** 026017 URL <https://dx.doi.org/10.1088/1741-4326/ac3b8b>
- ⁹Isler R C, McKee G R, Brooks N H, West W P, Fenstermacher M E and Wood R D 1997 *Physics of Plasmas* **4** 2989–2996 ISSN 1070-664X (Preprint https://pubs.aip.org/aip/pop/article-pdf/4/8/2989/12482685/2989.1_online.pdf) URL <https://doi.org/10.1063/1.872432>
- ¹⁰Stangeby P, Elder J, Boedo J, Bray B, Brooks N, Fenstermacher M, Groth M, Isler R, Lao L, Lisgo S, Porter G, Reiter D, Rudakov D, Watkins J, West W and Whyte D 2003 *Journal of Nuclear Materials* **313-316** 883–887 ISSN 0022-3115 plasma-Surface Interactions in Controlled Fusion Devices 15 URL <https://www.sciencedirect.com/science/article/pii/S0022311502014708>
- ¹¹Abrams T, Unterberg E A, Rudakov D L, Leonard A W, Schmitz O, Shiraki D, Baylor L R, Stangeby P C, Thomas D M and Wang H Q 2019 *Physics of Plasmas* **26** 062504 (Preprint <https://doi.org/10.1063/1.5089895>) URL <https://doi.org/10.1063/1.5089895>
- ¹²Na H, Sajjad S, Park J and Kwon M 2011 *Fusion Engineering and Design* **86** 66–70 ISSN 0920-3796 URL <https://www.sciencedirect.com/science/article/pii/S0920379610003625>
- ¹³Stephey L, Wurden G A, Schmitz O, Frerichs H, Effenberg F, Biedermann C, Harris J, König R, Kornejew P, Krychowiak M and Unterberg E A 2016 *Review of Scientific Instruments* **87** 11D606 (Preprint <https://aip.scitation.org/doi/pdf/10.1063/1.4959274>) URL <https://aip.scitation.org/doi/abs/10.1063/1.4959274>
- ¹⁴Xu Z, Wu Z W, Gao W, Chen Y J, Wu C R, Zhang L, Huang J, Chang J F, Yao X J, Gao W, Zhang P F, Jin Z, Hou Y M and Guo H Y 2016 *Review of Scientific Instruments* **87** 11D429 URL <https://aip.scitation.org/doi/abs/10.1063/1.4961294>
- ¹⁵Unterberg E A, Garren E W, Davda K M, Neff A L, Ray H R and Fehling D T 2019 The filterscope: A technical guide & user's manual URL <https://www.osti.gov/biblio/1615788>
- ¹⁶MDSplus URL <https://www.mdsplus.org/>
- ¹⁷Brooks N H, Howald A, Klepper K and West P 1992 *Review of Scientific Instruments* **63** 5167–5169 (Preprint <https://doi.org/10.1063/1.1143469>) URL <https://doi.org/10.1063/1.1143469>
- ¹⁸Hamamatsu 2007 Photomultiplier tubes: Basics and applications URL https://www.hamamatsu.com/content/dam/hamamatsu-photonics/sites/documents/99_SALES_LIBRARY/etd/PMT_handbook_v3aE.pdf
- ¹⁹Johnson L C and Hinnov E 1973 *Journal of Quantitative Spectroscopy and Radiative Transfer* **13** 333–358 URL <https://www.sciencedirect.com/science/article/pii/0022407373900642>

This is the author's peer reviewed, accepted manuscript. However, the online version of record will be different from this version once it has been copyedited and typeset.
PLEASE CITE THIS ARTICLE AS DOI: 10.1063/5.0175421

²⁰Summers H P, Dickson W J, O'Mullane M G, Badnell N R, Whiteford A D, Brooks D H, Lang J, Loch S D and Griffin D C 2006 *Plasma Physics and Controlled Fusion* **48** 263 URL <https://doi.org/10.1088/0741-3335/48/2/007>

²¹Fenstermacher M E, Meyer W H, Wood R D, Nilson D G, Ellis R and Brooks N H 1997 *Review of Scientific Instruments* **68** 974–977 URL <https://doi.org/10.1063/1.1147729>